WIND TURBINE EMULATOR FOR ENERGY QUALITY STUDIES

Matheus Martins, Rodrigo Z. Azzolin, Humberto Pinheiro
Universidade Federal de Santa Maria – Grupo de Eletrônica de Potência e Controle
Avenida Roraima, n° 1000 – Santa Maria – RS – Brasil
matmartins@gmail.com, rodrigoazzolin@gmail.com, humberto@ctlab.ufsm.br

***Abstract* – This paper describes a wind turbine emulation setup to evaluate the impact of different wind turbine concept on the grid. The wind turbine dynamics is reproduced by means of static and dynamic models using an induction motor servo system. The mechanical drive train dynamics as well as the tower shadow are well reproduced by the induction servo motor system. Several experimental results from a 5 kW generator connected to the grid are presented to demonstrate the performance of the implemented system. In addition, it is demonstrated the proposed implementation is suitable to investigate experimentally the impact of wind turbine generators on the grid voltage quality.**

***Keywords* – Wind Turbine, Induction Motor, Induction Generator.**

I. INTRODUCTION

In recent years, wind power generation has experienced a very fast development. As the wind power penetration into the grid is increasing quickly, the influence of wind turbines on the energy quality is becoming an important issue.

Power fluctuation in wind turbines occurs due to the stochastic nature of the wind speed and wind energy conversion system dynamics. The power oscillations are transmitted to voltage on point of common coupling (PCC) in weak grids. This problem is known as flicker [7].

The wind generation systems can be divided into two large groups: the fixed speed systems where usually squirrel cage induction generators (SCIG) are employed; and the variable speed systems, where doubly fed induction generators or synchronous generators are predominant [9], [14].

Constant speed wind turbines produce stochastic as well as periodic power fluctuations. The dominant periodic components have a frequency around 1 – 2 Hz. The resulting voltage fluctuations in weak grids can deteriorate the energy quality [8].

Variable speed wind turbines with doubly fed induction generator as well as synchronous generator are capable of controlling the output active and reactive power independently [10]. Then, the reactive power can be used to reduce flicker emission.

For the design of generator control systems, including protection and start-up circuits as well as pitch controllers and maximum power point tracking (MPPT) algorithms, a laboratory set up for validation of the control strategies is of fundamental importance.

A variety of configurations of wind turbine emulators have been reported in the literature, [1] – [6], however, in these works the authors suggest emulators that reproduce only the steady state conditions of the wind generation system or utilize torque control in the drive of the primary machine to emulate transitory conditions, [4] and [6]. However, in the last case, it is only possible to emulate low power turbines, because the inertia of the emulated system and experimental setup must be equivalents. Hence, important aspects such generated energy quality cannot be evaluated for high power wind turbines.

This paper describes an implemented wind turbine emulator that reproduces the steady state and dynamic conditions of operation of a real wind energy conversion system (WECS). The system is composed by a squirrel cage induction motor (SCIM) mechanically coupled to studied generator. The motor drive is a digital signal processor (DSP) based field oriented three phase power module. This processor makes a real time simulation of the turbine. The speed reference for speed servo control loop of primary machine is obtained from numerical solution of the wind turbine dynamic model.

Figure 1 shows the block diagram of described system. The static equation block has as inputs the turbine speed, wind speed and pitch angle. This block computes the aerodynamic torque considering the torque pulsations due to tower shadow. Per unit aerodynamic torque and generator measured torque are the inputs to drive train dynamic model, as results, the emulated turbine speed is used as speed reference for the SCIM control. In this way the wind turbine static and dynamic conditions of operation are emulated by the SCIM.

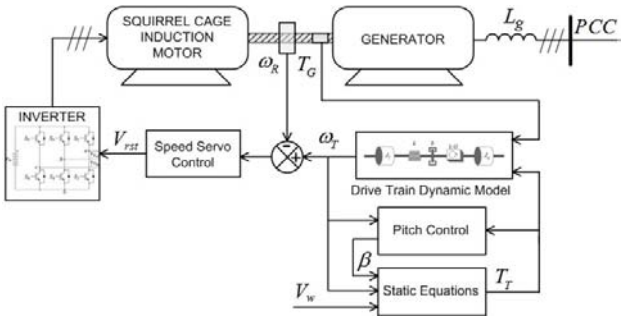

Fig. 1. Block diagram of proposed system.

The SCIM speed control is implemented in the synchronous coordinates at rotor flux reference frame. The indirect field oriented control (IFOC) has been selected, since this configuration has much better dynamic behavior then scalar control with comparable implementation simplicity.

Section II describes the wind turbine model. The speed servo design is presented in section III. Section IV

experimental results are shown and finally, in section V, conclusions and suggestion for future works are given.

II. WIND TURBINE MODEL

The aim of the implemented emulator is to evaluate the impact of high power WECS in distribution and transmission systems. These high power WECS have sufficiently large time constants and consequently a servo system with a bandwidth of few hertz can emulate it behavior under different operating conditions.

The turbine model has three inputs: the wind speed, stored at DSP memory; rotational speed and torque measured from the shaft of the experimental setup.

The wind turbine model considers the static and dynamic behavior of the system. The static equation computes the instantaneous aerodynamic torque on the rotor shaft based on turbine speed, position, pitch angle and wind speed. This torque is subjected of effects of tower shadow and pitch control. The dynamic equation computes the turbine speed according to dynamic behavior of mechanical drive train. This dynamic equation has aerodynamic torque and generator torque as inputs.

A. Aerodynamics Static Equations

The power into air mass with density ρ with speed V_w, intercepted by a wind turbine with rotor area A is calculated:

$$P_w = \frac{1}{2}\rho A V_w^3 \quad (1)$$

The turbine efficiency is expressed as function of the ratio of between speed at the tip of the blade and the wind speed, that is:

$$\lambda = \frac{\omega_T R}{V_w} \quad (2)$$

The relation (2) is known as Tip Speed Ratio (TSR). The wind turbine manufacturers usually make available a curve with values of power coefficient for a range of TSR, where power coefficient is defined:

$$C_p(\lambda) = \frac{P_T}{P_w} \quad (3)$$

Thereby is possible to calculate the input aerodynamic power (P_T) and aerodynamic torque (T_T) as function of wind speed, turbine rotational speed and coefficient power curve using (1) – (3).

High power turbines usually have to limit the mechanical power to avoid mechanical stress in adverse conditions like wind gusts. Hence, mechanisms which enable longitudinal rotation on turbine blades are utilized to increase or decrease the efficiency on energy capture, depending on the necessity. This strategy is known as pitch control. Thereby the power coefficient also depends on pitch angle β [9]. Figure 2 shows the power coefficient curves as function of λ and β.

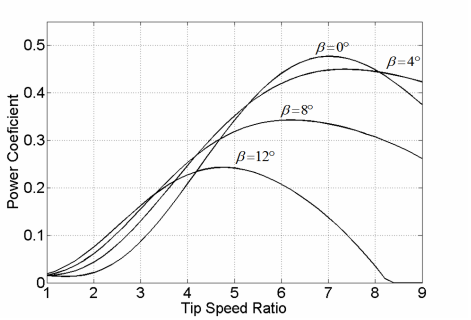

Fig. 2. Power Coefficient as function of λ and β.

Real time computation of the power coefficient is obtained from a look-up-table operation followed by a two dimensional interpolation. For this propose, 750 values of $C_P(\lambda,\beta)$ have been stored at DSP memory for a range of $0 < \lambda < 10$ and $0^o < \beta < 15^o$.

In high power wind turbines occurs a phenomenon that has direct impact on energy quality, known as tower shadow. Each time that a blade passes through the turbine tower, the torque in this blade is reduced.

Tower shadow originates oscillations on mechanical torque with multiplies frequencies of NP Hz where N is the turbine speed and P the number of blades of turbine [8]. Figure 3 illustrates this phenomenon where wind speed is constant. At figure 3(a) the torque in rotor blades is plotted as function of the rotor position. Figure 3(b) shows the harmonic content of the torque ripple generated by the tower shadow.

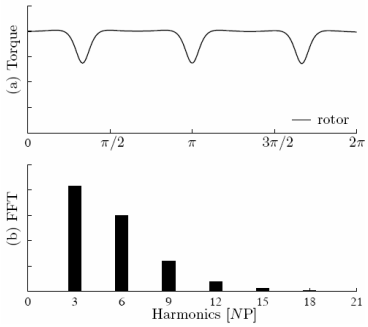

Fig. 3. Tower shadow: (a) torque as function of rotor position, (b) normalized FFT.

Usually the tower shadow is main cause of deterioration of generated energy quality. In addition, the harmonic frequencies showed in figure 3 can excite resonances in the mechanical drive train. These oscillations in turn can be transmitted to turbine speed and generated power, and, in weak grids, to the point of common coupling. As a result an increase in the light flicker emission can be expected.

Figure 4 shows the block diagram of turbine static equations. In this block, the mechanical torque is computed considering the tower shadow effect. The K_{sh} gain depends on turbine rotor position as well as shown on figure 3.

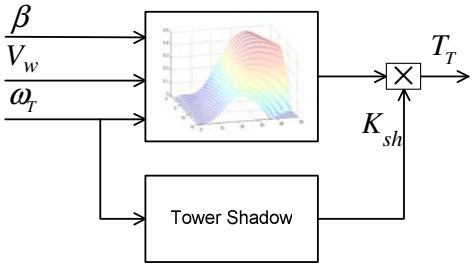

Fig. 4. Static equations block.

B. Drive Train Dynamic Model

The drive train dynamic model is composed by the turbine rotor and generator inertias (J_T , J_G), stiffness of the shaft (k) and damp (b), as shown in figure 5.

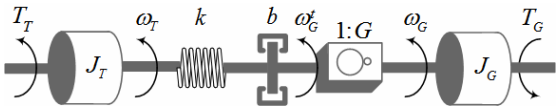

Fig. 5. Drive train equivalent mechanical model.

A gearbox with transformation ratio of G is used to couple the low speed side of turbine (left) with the high speed side of generator (right). For convenience, all system variables and parameters are referenced in the same base of speed and torque. Moreover, the power of emulated turbine can be much larger than the power of generator at experimental setup, therefore the emulated dynamic model must be given in per unit system (p.u.).

By referring all parameters and variables to the low speed side of gearbox, results:

$$T_G^t = GT_G \tag{4}$$

$$w_G^t = G^{-1} w_G \tag{5}$$

$$J_G^t = G^2 J_G \tag{6}$$

With (4) – (6), the gearbox shown in figure 5 is eliminated. Hence, the system can be described by:

$$\dot{J}_T w_T + T_k = T_T \tag{7}$$

$$\dot{J}_G^t w_G^t + b w_G^t + T_G^t = T_k \tag{8}$$

$$\dot{T}_k = k\left(w_T - w_G^t\right) \tag{9}$$

By rearranging (7) – (8) is possible to write:

$$\begin{bmatrix} \dot{\omega}_T \\ \dot{\omega}_G^t \\ \dot{T}_k \end{bmatrix} = \begin{bmatrix} 0 & 0 & \frac{-1}{J_T} \\ 0 & \frac{-b}{J_G^t} & \frac{1}{J_G^t} \\ k & -k & 0 \end{bmatrix} \begin{bmatrix} \omega_T \\ \omega_G^t \\ T_k \end{bmatrix} + \begin{bmatrix} \frac{1}{J_T} & 0 \\ 0 & \frac{-1}{J_G^t} \\ 0 & 0 \end{bmatrix} \begin{bmatrix} T_T \\ T_G^t \end{bmatrix} \tag{10}$$

The state equation (10) has parameters and variables in SI units. To obtain the per unit model, power and speed bases must be defined, then, other bases are given by:

$$T_{base}^t = \frac{P_{base}}{\omega_{base}^t} \tag{11}$$

$$\omega_{Gpu}^t = \frac{\omega_G^t}{\omega_{base}^t} \tag{12}$$

$$J_{base}^t = k_{base}^t = b_{base}^t = \frac{P_{base}}{\omega_{base}^{t\,2}} \tag{13}$$

Table I shows typical parameters for a wind turbine with rotor diameter of 52 meters and rated power of 1MW.

TABLE I
Turbine parameters

Parameter	SI	Per Unit
P_{base}	10^6 W	1
ω_{base}^t	3.1416 rad/s	1
T_{base}^t	318310 Nm	1
J_T	$6*10^5$ kgm^2	5.9218
J_G	180 kgm^2	6.3955
k	$3.6*10^6$ Nm/rad	35.5307
b	1000 Ns/rad	0.0099

The transfer function that relates the generator speed at low speed base (ω_G^t) with aerodynamic torque (T_T) is:

$$\frac{\omega_G^t(s)}{T_T(s)} = \frac{1/J_G^t \left(s^2 + b/J_T\, s + k/J_T\right)}{s^3 + b/J_T\, s^2 + \left(k/J_T + k/J_G^t\right)s + bk/J_T J_G^t} \tag{14}$$

Figure 6 shows a bode diagram of (14).

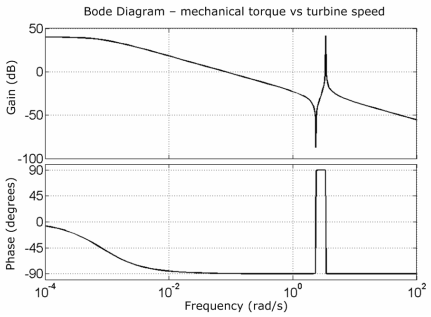

Fig. 6. Bode diagram of drive train mechanical model.

In the frequency response of the emulated dynamic system exists a resonance peak on 3,4 rad/s. This resonance frequency depends of the parameters of the emulated turbine, where, largest power turbines have lowest resonance frequency and vice-versa.

In order to reproduce this behavior the bandwidth of the speed servo system has been set to 60 rad/s. The details of the IFOC servo system are seen in the next section.

III. SPEED SERVO DESIGN

In [1], [3], [4] and [5], d.c. motors are used as primary machine to wind turbine emulator. This type of motor has excellent dynamic behavior and is simple to control. However this is expensive and needs periodical maintenance. In [2], a SCIM is utilized, but dynamic behavior of the drive train is not emulated, then a simplified model and a scalar control strategy are utilized.

In this paper, an IFOC has been implemented. Initially, the synchronous coordinates SCIM model at rotor flux reference frame are derived. Then, the controllers to compensate the q and d axis currents coupling are presented. Finally, speed control loop controller is described.

A. Squirrel Cage Induction Motor modeling

The αβ electric model of the machine is given by (15) – (18), [12].

$$\begin{bmatrix}\lambda_{s\alpha}\\ \lambda_{s\beta}\end{bmatrix}=L_{ss}I_{2x2}\begin{bmatrix}i_{s\alpha}\\ i_{s\beta}\end{bmatrix}+L_M\begin{bmatrix}\cos(\theta_R) & -\sin(\theta_R)\\ \sin(\theta_R) & \cos(\theta_R)\end{bmatrix}\begin{bmatrix}i_{r\alpha}\\ i_{r\beta}\end{bmatrix} \quad (15)$$

$$\begin{bmatrix}\lambda_{r\alpha}\\ \lambda_{r\beta}\end{bmatrix}=L_{rr}I_{2x2}\begin{bmatrix}i_{r\alpha}\\ i_{r\beta}\end{bmatrix}+L_M\begin{bmatrix}\cos(\theta_R) & \sin(\theta_R)\\ -\sin(\theta_R) & \cos(\theta_R)\end{bmatrix}\begin{bmatrix}i_{s\alpha}\\ i_{s\beta}\end{bmatrix} \quad (16)$$

$$\begin{bmatrix}v_{s\alpha}\\ v_{s\beta}\end{bmatrix}=\begin{bmatrix}r_s & 0\\ 0 & r_s\end{bmatrix}\begin{bmatrix}i_{s\alpha}\\ i_{s\beta}\end{bmatrix}+\begin{bmatrix}\dot{\lambda}_{s\alpha}\\ \dot{\lambda}_{s\beta}\end{bmatrix} \quad (17)$$

$$\begin{bmatrix}v_{r\alpha}\\ v_{r\beta}\end{bmatrix}=\begin{bmatrix}r_r & 0\\ 0 & r_r\end{bmatrix}\begin{bmatrix}i_{r\alpha}\\ i_{r\beta}\end{bmatrix}+\begin{bmatrix}\dot{\lambda}_{r\alpha}\\ \dot{\lambda}_{r\beta}\end{bmatrix} \quad (18)$$

By applying the Park transformation for stator and rotor equations, (19) – (20), it is possible decouple machine fluxes equations, (22) – (23):

$$\mathbf{B}_S^{-1}(\beta)=\mathbf{B}_S(\beta)=\begin{bmatrix}-\sin(\beta) & \cos(\beta)\\ \cos(\beta) & \sin(\beta)\end{bmatrix} \quad (19)$$

$$\mathbf{B}_R^{-1}(\gamma)=\mathbf{B}_R(\gamma)=\begin{bmatrix}-\sin(\gamma) & \cos(\gamma)\\ \cos(\gamma) & \sin(\gamma)\end{bmatrix} \quad (20)$$

$$\gamma=\beta-N\theta_R,\ \beta=\int\omega dt \quad (21)$$

$$\begin{bmatrix}\lambda_{qs}\\ \lambda_{ds}\end{bmatrix}=\begin{bmatrix}L_{ss} & 0\\ 0 & L_{ss}\end{bmatrix}\begin{bmatrix}i_{qs}\\ i_{ds}\end{bmatrix}+\begin{bmatrix}L_M & 0\\ 0 & L_M\end{bmatrix}\begin{bmatrix}i_{qr}\\ i_{dr}\end{bmatrix} \quad (22)$$

$$\begin{bmatrix}\lambda_{qr}\\ \lambda_{dr}\end{bmatrix}=\begin{bmatrix}L_{rr} & 0\\ 0 & L_{rr}\end{bmatrix}\begin{bmatrix}i_{qr}\\ i_{dr}\end{bmatrix}+\begin{bmatrix}L_M & 0\\ 0 & L_M\end{bmatrix}\begin{bmatrix}i_{qs}\\ i_{ds}\end{bmatrix} \quad (23)$$

If the frequency base ω_b is defined then it is possible to obtain the per unit machine model where inductances and flux are substituted by:

$$X_{ij}=\omega_b L_{ij} \quad (24)$$

$$\psi_{ij}=\omega_b\lambda_{ij} \quad (25)$$

Applying the Park transform on (17) – (18) and substituting (22) – (23) taking into account (24) – (25) makes the per unit synchronous coordinates electrical model.

Rotor flux reference frame is obtained when synchronous speed is computed by:

$$\omega=N\omega_R+\omega_b\left(r_r\, i_{qs}/X_{rr}\, i_{ds}\right) \quad (26)$$

Replacing (26) on obtained electrical model and applying the Laplace transform gives the transfer functions to q and d axis currents:

$$\frac{i_{qs}(s)}{v_{qs}(s)-\frac{D}{X_{rr}}\frac{\omega}{\omega_b}i_{ds}(s)}=\frac{1}{\frac{D}{X_{rr}\omega_b}s+r_s} \quad (27)$$

$$\frac{i_{ds}(s)}{v_{ds}(s)+\frac{D}{X_{rr}}\frac{\omega}{\omega_b}i_{qs}(s)}=\frac{1}{s\frac{D}{\omega_b X_{rr}}+r_s} \quad (28)$$

Where: $D=X_{ss}X_{rr}-X_M^2$.

Table II shows the parameters of the SCIM.

TABLE II
SCIM parameters

L_m	57.75mH
$L_{ls}=L_{lr}$	2.2mH
R_s	0.47Ω
R_r	0.26Ω
J	0.124 kgm^2
b	0.0113 Ns/rad

B. Speed Control Design

The currents coupling evidenced in (27) and (28) can be compensated by proportional-integral controllers (PI), in this way, the controllers gains are designed to electrical loop achieve the bandwidth of ten times desired bandwidth of mechanical control loop. Figure 7 presents a block diagram of described currents control loop.

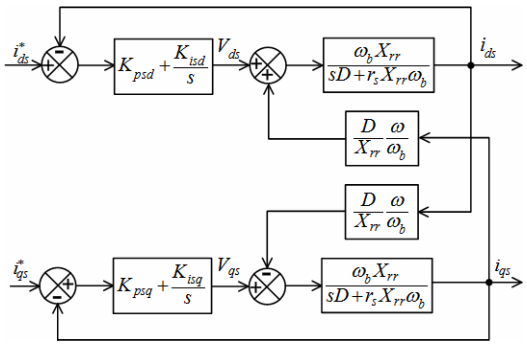

Fig. 7. SCIM current control loop.

In this reference frame, the electrical torque is computed by:

$$T_{IM}=K_{TN}i_{qs} \quad (29)$$

$$K_{TN}=\frac{3}{2}N\frac{X_M\psi_{dr}}{X_{rr}} \quad (30)$$

The electrical torque is directly proportional to q axis stator current, while the magnetization is directly

proportional to d axis stator current. If i_{ds} is constant then $\psi_{qr} = 0$ and:

$$\psi_{dr} = X_M i_{ds} \tag{31}$$

The transfer function of mechanical part is:

$$G_m(s) = \frac{\omega_R(s)}{i_{qs}(s)} = \frac{K_{TN}/J_m}{s + b_m/J_m} \tag{32}$$

Finally, a PI controller have been utilized in the closed loop, where its bandwidth have been selected 60 rad/s. Figure 8 shows the block diagram of the speed control loop.

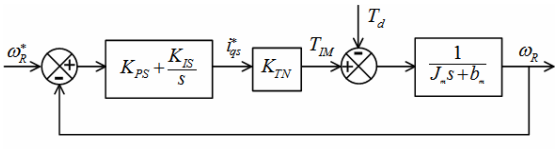

Fig. 8. SCIM speed control loop.

IV. EXPERIMENTAL RESULTS

The speed servo was implemented in a three phase PWM inverter module [11]. This is composed by: protection and start-up circuits, instrumentation and control block, power supplies, three leg PWM inverter, crowbar resistors for d.c. bus discharge and protection.

The power module has a development kit *F2812 eZdsp starter kit*, manufactured by *Spectrum Digital*. This kit has a TMS320F2812 DSP manufactured by *Texas Instruments*. This processor has a 32 bits word length fixed point arithmetic and dedicated modules for machine drives applications.

A two bits quadrature encoder pulse (qep) with 300 lines resolution was used for measurement of rotor position and speed compute. The shaft torque is measured by TorqueTrak 9000 system manufactured by *Binsfeld*.

A 5kW wounded rotor induction generator with short-circuit rotor was utilized as a squirrel cage induction generator (SCIG). Then an emulation of a fixed speed wind turbine with parameters in Table I was performed. Figure 9 shows a picture from experimental setup.

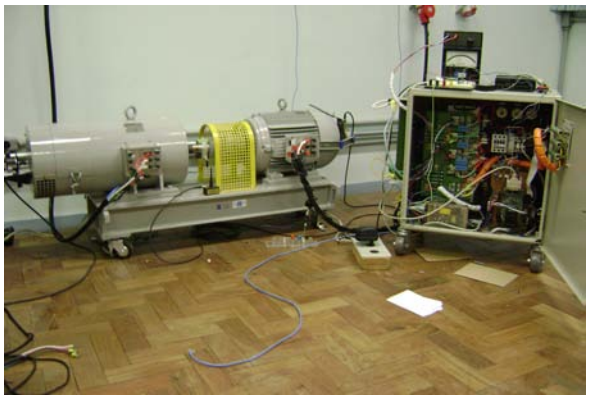

Fig. 9. Experimental setup.

Figure 10 shows the wind speed time series implemented.

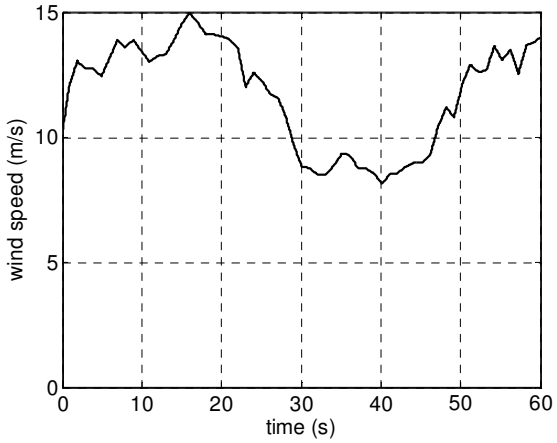

Fig. 10. Wind speed.

Figure 11 shows the aerodynamic torque and the generator torque measured at generator shaft.

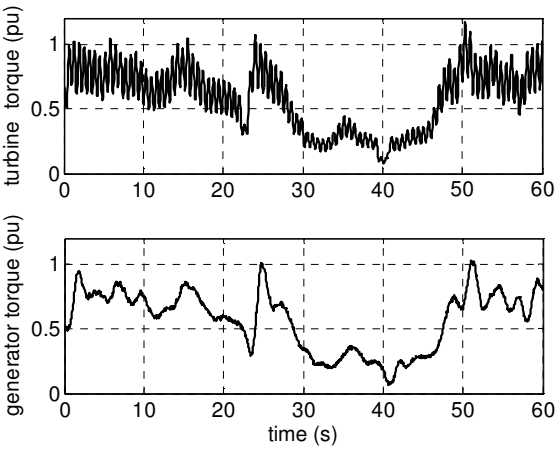

Fig. 11. Aerodynamic torque.

Figure 12 shows the power coefficient from static equation block and pitch angle from pitch control block.

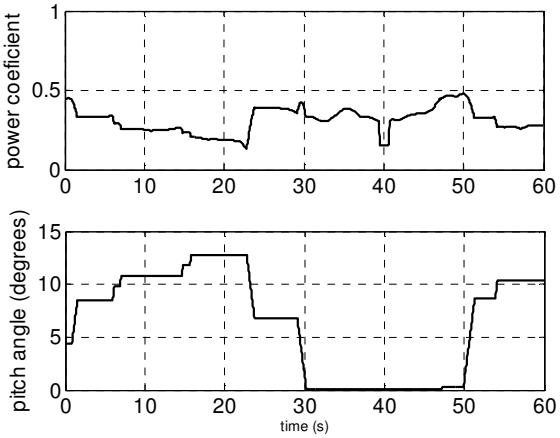

Fig. 12. Power Coefficient (C_p) and pitch angle (β) .

Figure 13 shows the resulting measured generator speed and reference speed obtained from real time wind turbine simulation. Figure 14 shows a zoom view of figure 13.

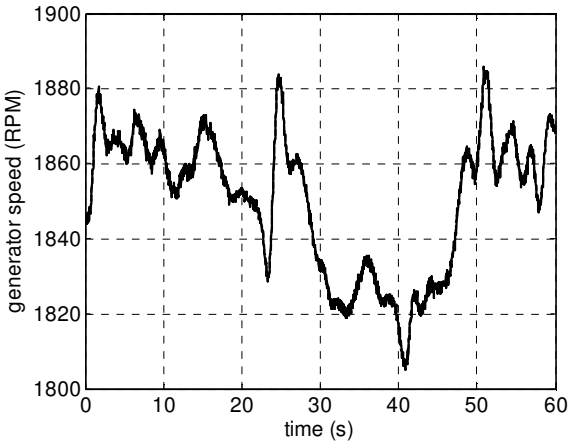

Fig. 13. Generator speed (servo reference, from real-time simulation) and measured servo speed.

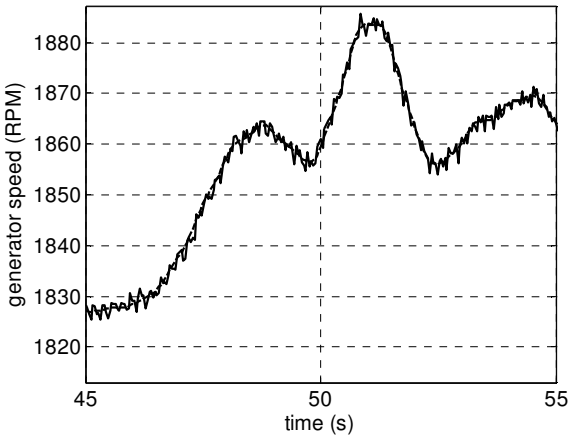

Fig. 14. Generator speed (servo reference, from real-time simulation) and measured servo speed (zoom).

V. CONCLUSIONS

In this paper a new approach for wind turbine emulation setup was presented. With this configuration it is possible to emulate different power wind generation systems according to bandwidth of speed servo, where, smallest wind turbines need highest speed servo bandwidth and vice versa.

With this system, experimental validation of grid connected generator control systems can be obtained. Furthermore, performance figures like flicker coefficients can be obtained for grid code compatibility tests.

REFERENCES

[1] P. E. Battaiotto, R. J. Mantz, P. F. Puleston, "A Wind Turbine Emulator Based on a Dual DSP Processor System", *Control Eng. Practice*, vol. 4, no. 9, pp. 1261-1266, 1996.

[2] H. M. Kojabadi, L. Chang, T. Boutot, "Development of a Novel Wind Turbine Simulator for Wind Energy Conversion Systems Using an Inverter-Controlled Induction Motor", *IEEE Transactions on energy conversion*, vol. 19, no. 3, pp. 547-552, September 2004.

[3] M. Chinchilla, S. Arnaltes, J. L. Rodriguez-Amenedo, "Laboratory Set-up for Wind Turbine Emulation", *IEEE International Conference on Industrial Technology*, vol. 1, no. 8, pp. 553-557, December 2004.

[4] L. A. C. Lopes, J. Lhuilier, A. Muherjee, M. F. Khokhar, "A Wind Turbine Emulator that Represent the Dynamics of the Wind Turbine and Drive Train", *IEEE Power Electronics Specialists Conference*, pp. 2092-2097, 2005.

[5] B. Rabelo, W. Roffman, M. Gluck, "Emulation of Static and Dynamic Behavior of a Wind Turbine with a DC-Machine Drive'", *IEEE Power Electronics Specialists Conference*, vol. 3, pp. 2107-2112, June 2004.

[6] R. Teodoresco, F. Iov, F. Blaabjerg, "Flexible Development and Test System for 11kW Wind Turbine", *IEEE Power Electronics Specialists Conference*, vol. 1, pp. 67-72, June 2003.

[7] T. Sun, Z. Chen, F. Blaabjerg, "Flicker Study on Variable Speed Wind Turbines with Doubly Fed Induction Generators", *IEEE Transactions on energy conversion*, vol. 20, no. 4, pp. 896-905, December 2005.

[8] T. Thiringer, J. Dahlberg, "Periodic Pulsations from a three Bladed Wind Turbine", *IEEE Transactions on energy conversion*, vol. 16, no. 2, pp. 128-133, June 2001.

[9] J. Marques, H. Pinheiro, "Turbinas Eólicas: Modelo, Análise e Controle do Gerador de Indução com Dupla Alimentação", Master Thesis, Power Electronics and Control Research Group, Federal University of Santa Maria, 2004.

[10] J. P. da Costa, H. Pinheiro, "Contribuição ao Estudo da Máquina Assíncrona Trifásica Duplamente Alimentada Aplicada a Aerogeradores de Velocidade Variável", Master Thesis, Power Electronics and Control Research Group, Federal University of Santa Maria, 2006.

[11] R. Z. Azzolin, "Desenvolvimento de uma fonte de potência C.A. para acionamento e controle de máquinas elétricas", conclusion course project report, Power Electronics and Control Research Group, Federal University of Santa Maria, 2006.

[12] P. C. Krause, "Analysis of electrical machinery", McGraw-Hill Book Company, 1986.

[13] V. Gasparetto, "Estudo de Dispositivos de Controle de Turbinas Eólicas", Research Report, , Power Electronics and Control Research Group, Federal University of Santa Maria, 2005.

[14] T. Nakamura, S. Morimoto, M. Samada, Y. Takeda, "Optimum control of IPMSG for wind generation system", *Power Conversion Conference*, vol. 3, pp. 1435-1440, 2002.

[15] L. M. Popa, F. Blaabjerg, I. Boldea "Wind turbine generator modeling and simulation where rotational speed is the controlled variable", *IEEE Trans. On industry applications.* vol. 40, no. 1, January 2004.